Sum Frequency Generation Microscopy of Microcontact-Printed Mixed Self-Assembled Monolayers

Katherine Cimatu and Steven Baldelli*

Department of Chemistry, University of Houston, Houston, Texas 77204

Received: October 31, 2005; In Final Form: December 10, 2005

Sum frequency generation imaging microscopy (SFGIM) is used to image the chemically distinct regions of a microcontact-printed monolayer surface. The contrast in the images is based on the vibrational spectrum of each component in the monolayer. Mixtures of C_{16} thiols on gold with CH_3 and phenyl termination are imaged with a resolution of ~10 μm. Microcontact printing produces films that are different compared to the immersion procedure of forming self-assembled monolayers. The SFGIM technique is able to obtain a vibrational spectrum at each point on the surface and demonstrate that the stamped area has significant mixing with the molecules deposited from the backfilling solution.

Introduction

Self-assembled monolayers (SAMs) continue to be an interesting area of study and research.[1] SAMs are characterized by measuring wettability (contact angle) properties, refractive index, thickness, atomic and molecular structure, chemical composition, and response to formation on different substrates. This type of detailed information is important for SAMs when used in applications of microcontact printing in the field of microelectronics, biological systems and structures, microelectromechanical systems, microanalytical systems, sensors, solar cells, and optical systems.[2] Microcontact printing has become an extremely valuable technique to researchers in many fields who desire spatial control over the chemical properties of a surface.

As an example, microcontact printing (or soft lithography) has been useful in the field of microelectronics in the formation of ultrathin resists.[3] In microelectronics, semiconductors are used to make small electronic components used in digital integrated circuits using photolithography processes. Due to development demands, alternative processes have been sought to modify and improve the production of these microstructure devices, such as electron beam writing, photoactivation, micromachining, and microcontact printing.

Another application uses soft lithography for patterning of cell-adhesive SAMs.[4] Because the head and end groups of the molecules can be modified and replaced with other functional groups, the interfacial properties, such as the wettability, of SAMs can be varied systematically. This fact, with the spatial control of microcontact printing, is able to specifically locate molecules on the surface. Thus, modified SAMs on Au can be used as good substrates to study the properties of the biological cells after attachment.[2]

The characterization of surfaces is an active area of research. Many techniques have been developed over the past few decades to obtain chemical, structural, and spatial information, in situ, about surfaces and interfaces. Some techniques are good for one or two of the above-mentioned criteria but seldom are all four met. Solid surfaces are typically heterogeneous in two dimensions, and it is therefore critical to account for this heterogeneity to understand surface chemistry. This is especially important in materials characterization and biological systems. A few techniques have been developed recently that are able to probe solid surfaces in situ with chemical specificity, monolayer sensitivity, and spatial resolution with at least micrometer resolution,[5−9] notably, atomic force microscopy (AFM) or its derivatives of chemical force microscopy (CFM) and lateral force microscopy (LFM).[10] These techniques are able to obtain contrast based on the chemical functionality of the monolayer and its relation to friction or adhesion.[11] Also, synchrotron-based X-ray techniques are becoming useful for probing solid surfaces with good spatial resolution.[12,13]

This paper describes the preparation of SAMs of *n*-alkanethiolates formed by microcontact printing (μCP), addition of another SAM by immersion after printing (backfilling), and characterization of the SAMs formed on gold using a newly developed sum frequency generation microscope. This system is also ideal for testing the capability of this new microscopy method by acquiring specific spectra using the unprocessed images of the interface scanned from 2800 to 3150 cm^{-1}, observing the contrast of the image as the wavenumber changes, and obtaining the spatial resolution of the SFG microscope setup and distribution of molecules on the surface.

Background

Microcontact printing as pioneered by Whitesides is a versatile and convenient method of creating spatial functionality on a surface.[14] This process involves creating a patterned stamp onto which the ω-functionalized alkanethiol molecules are inked. The stamp typically consists of poly(dimethylsiloxane) (PDMS) with known chemical and mechanical properties.[15] Next, the inked stamp is put into contact with the surface (usually gold), and the thiols are transferred from the stamp to the surface in the complementary patterned way that accurately reflects the stamp's pattern.[14] The mechanism of this process has been discussed in detail, and conditions for optimization have also been identified.[16] The specifics of the process are complicated, and the resolution of the pattern is determined by the relative rates of gas-phase diffusion from the stamp to the gold, the diffusion of thiol in PDMS,[16] and the rate of monolayer formation vs the spreading of the liquid.[17] While microcontact printing has been widely used and successful in many applica-

* To whom correspondence should be addressed. E-mail: sbaldelli@uh.edu.

10.1021/jp0562779 CCC: $33.50
Published on Web 01/11/2006

tions, there are still questions on the structure of the formed monolayer in the pattern, the stability of the film, and the structure at the pattern's boundary.[18] To resolve the issues in microcontact printing requires a technique that is highly sensitive, interface specific, and provides chemical/structural information with good spatial resolution.

In recent years, imaging based on nonlinear optical processes has become a viable and useful technique. Far-field microscopy based on second harmonic generation (SHG)[19−25] and coherent anti-stokes Raman spectroscopy (CARS)[26−30] has been particularly effective at probing material surfaces and biological molecules. Since SHG is a second-order nonlinear technique, it is surface sensitive due to the inherent breaking of symmetry at the interface and typically provides electronic structure information, while CARS is valuable since it provides a spatially resolved vibrational spectrum of the system. However, CARS, based on a third-order nonlinear process, is not surface specific. Recently, images of a surface monolayer were achieved using sum frequency generation (SFG) microscopy by Kuhnke et al.[31,32] and Florsheimer.[33,34]

SFG is a nonlinear vibrational spectroscopy technique that is used to detect molecules at the surface of a material. The technique involves overlapping two pulsed laser beams at the surface: one visible beam and one frequency tunable IR beam, creating a third beam with a frequency that is the sum of the two input frequencies. When the IR light comes into resonance with a surface vibrational mode, there is an increase in the nonlinear susceptibility, $\chi^{(2)}$, and in related to the SFG intensity, I_{SF}, which is defined as follows

$$I_{SF} \propto |\sum_{JK} \chi_{IJK}{}^{(2)} E_J(\omega_{vis}) E_K(\omega_{IR})|^2 \quad (1)$$

where $\chi_{IJK}{}^{(2)}$ is the second-order nonlinear surface susceptibility and the $E(\omega)$ terms are light field amplitudes. The tensor, $\chi_{IJK}{}^{(2)}$, contains the information related to the interfacial structure. The resonant portion contains the vibrational information of the molecules, $\chi_R{}^{(2)}$, while the nonresonant susceptibility is due primarily to the gold substrate, $\chi_{NR}{}^{(2)}$

$$\chi^{(2)} = \chi_R{}^{(2)} + \chi_{NR}{}^{(2)} = \sum_q \frac{A_q}{\omega_{IR} - \omega_q + i\Gamma} + \chi_{NR}{}^{(2)} \quad (2)$$

where ω_{IR} and ω_q are the IR frequency and the resonant frequency of the qth vibrational mode, respectively. The damping factor of the vibration is Γ. The A_q term contains information on the IR and Raman transition moments

$$\chi_R \propto N\langle\beta\rangle \quad (3)$$

where N is the number of molecules generating signal and $\langle\beta\rangle$ is the orientational averaged hyperpolarizability, which is the product of the IR and Raman transition moments.

Because SFG is a $\chi^{(2)}$ process, a signal is only generated in a medium that lacks inversion symmetry, such as the surface. Therefore, a plot of IR wavelength vs sum frequency intensity is interpreted as the vibrational spectrum of the molecules on the surface. Due to phase matching conditions, SFG output is directional, which allows for the efficient collection of signal photons.[35,36] The phase-matching condition is also responsible for the lateral resolution of surface features, which is important for the imaging method. The orientation of the molecules at the surface can be determined by varying the polarization of the light fields that probe the sample. Since the sum frequency signal is coherent, the phase of the signal can be used to determine the sign of the susceptibility, which indicates whether the functional group is directed up or down at the surface.[37,38]

Experimental Section

Materials. Chemicals for the preparation of the monolayers were either purchased or obtained from T. R. Lee group (University of Houston). The reagents used are hexadecane-1-thiol and 16-phenylhexadecane-1-thiol. Hexadecane-1-thiol from TCI was used as received. The preparation of 16-phenylhexadecane-1-thiol is in the literature.[39] The solvent used was absolute ethanol (AAper).

Procedure for Making Patterns. A. Preparation of the Gold Substrate. Si(100) wafers were cleaned with absolute ethanol before attachment to a rotating plate in the evaporator. The gold substrates used for the formation of the SAM were prepared by evaporating 100 nm gold onto Si(100) wafers, which were precoated with a 10 nm chromium adhesion layer. After the gold deposition, the quality of the Au film was evaluated by ellipsometry.

B. Preparation of the PDMS Stamp/Pattern. The PDMS stamp was prepared by pouring and mixing a 10:1 ratio of SYLGARD 184 and the curing agent into a clean, dry beaker. The PDMS prepolymer was poured onto the specified patterned master used for each experiment and was cured at ∼150° for 15 min to remove the bubbles and to ensure complete polymerization. The mold was cooled to room temperature, and the PDMS mold was slowly removed by hand, rinsed with ethanol, and dried with nitrogen gas.

C. Process of Microcontact Printing (μCP). The gold substrate was thoroughly rinsed with absolute ethanol and dried under a stream of nitrogen gas. The PDMS stamp was dipped for a few seconds into the respective 1 mM alkanethiolate ($HS-(CH_2)_{15}-X$, (A) $X = CH_3$, (B) X = phenyl) solution in ethanol and dried with nitrogen gas. The PDMS stamp with thiols was gently applied to the gold substrate. A slight pressure was applied to the PDMS stamp and left in contact with the substrate for about 5 min. After careful removal of the stamp, the gold substrate was backfilled with another thiol solution (1 mM) and was left for about 5−10 min to allow the second monolayer to form. The sample was taken out of the solution and was rinsed thoroughly with absolute ethanol then dried under a stream of nitrogen gas. This procedure is adapted from that of Larsen et al. who demonstrated that these deposition times form dense, well-ordered monolayers.[16]

D. Description of the Laser System and Microscope. A picosecond pulsed Nd:YAG laser (EKSPLA) with a 20 Hz repetition rate was used in the following set of experiments.[40] The Nd:YAG laser pumps the optical parametric generator/amplifier (OPG/OPA) to generate the IR beam, which is tunable from 1000 to 4000 cm^{-1}. Both a 1064 nm and IR beam were used to probe the surface. These two beams were used in the setup for generating the SFG signal.

The incident angles of the IR and 1064 nm beams at the surface, as shown in Figure 1 were 70.0° and 60.0°, respectively. It was necessary to make sure that both beams overlap at the same time and space to generate the SFG signal. The beams were set to p-polarization. The angle of the output SFG signal was close to the angle of the 1064 nm beam, which was calculated to be 62.1°. No polarizer was placed at the output to select the polarization of the SFG signal. An interference filter was positioned after the sample to attenuate the 1064 nm signal. Two camera lenses were positioned to project an intermediate image of the sample (SFG signal) onto the grating. Another interference filter was placed after the lenses to prevent the 532

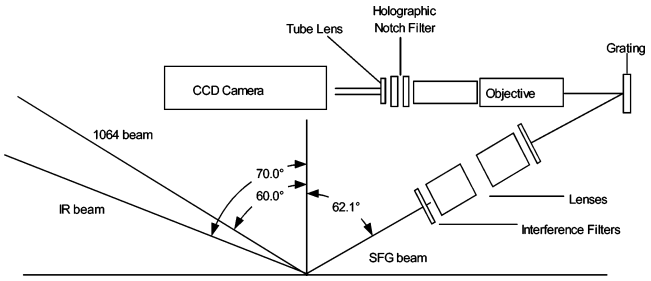

Figure 1. Optical setup of the SFG microscope (reflection configuration).

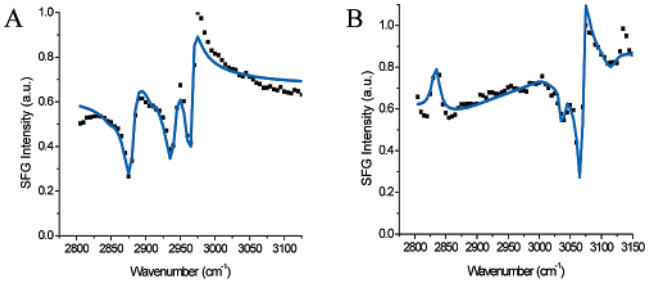

Figure 2. SFG spectra of solution prepared $S-(CH_2)_{15}-X$ monolayers on a gold surface, (A) X = CH_3, (B) X = phenyl. Prepared by immersion in 1 mM solution for 18 h. All spectra are in pp (1064 and IR) polarization combination.

nm (from SHG) going through the detection system. The holographic reflective grating was attached to the setup where it diffracts the SFG signal coming from the sample into the microscope. The microscope setup was positioned perpendicular to the intermediate image from the grating. It has a 10x objective lens, which magnifies the intermediate image, and a tube lens for collimation. The 532 and 1064 nm holographic notch filters were inserted in the microscope setup to attenuate further the intensity of the 532 and 1064 beams.[31] A Roper 1024 × 1024 pixel array CCD camera is the detector.

E. Collection and Processing of the Data. Images and spectra were obtained by continuously scanning the IR at a set scan rate and averaging the SFG signal over a range of 5 cm^{-1} intervals. Images were background corrected but no other processing was performed on the presented images. Spectral data were obtained by averaging the pixels of a given area at a specific wavelength and plotting the results in Origin software. Typical acquisitions were 1000−5000 shot/point or less, which is equivalent to 0.82−4.1 min per data point (wavelength). Spectra are curve fit using eq 2 for the analysis of peak amplitude, wavenumber, and width. This analysis is presented as the solid line in Figure 2, Figure 4, and Figure 6, respectively.

Results and Discussion

The results presented here suggest three important conclusions. First, SFG is able to obtain spatially resolved vibrational spectra of monolayers. The molecules in the stamped patterned surface appear to be mixed with the backfilled molecules. The results also indicate that the molecules at the edge of the pattern are more disordered that those in the middle of the patterned region.

Figure 2 shows the SFG spectra of pure monolayers of methyl- and phenyl-terminated C_{16} alkanethiols on gold. The spectra were acquired with the SFG microscope by integration of the entire laser spot from 2800 to 3150 cm^{-1}. The spectra indicate well-ordered monolayers for the CH_3 and phenyl films. As shown, the spectrum shape is different than what is normally presented in the literature due to the use of a 1064 nm wavelength instead of 532 nm for the pump beam. This is a result of the different nonlinear optical factors at the surface of gold at 532 and 1064 nm as discussed by Bain.[41,42] These spectra serve a reference for interpreting the patterned surfaces. Three main peaks are observed in Figure 2A, at 2875, 2935, and 2965 cm^{-1}, and are assigned to the symmetric stretch, Fermi resonance, and the antisymmetric stretch of the terminal methyl group.[43−45] The peaks at ∼3060 cm^{-1} in Figure 2B of the phenyl-terminated SAM are due to the aromatic C−H stretch of the phenyl ring.[46,47]

Checkerboard patterned thiols are shown in Figure 3. The features in the pattern are 100 × 100 μm. All the images were taken on the same spot by tuning the IR to different frequencies, ranging from 2800 to 3150 cm^{-1}. The sample was stamped with 1-hexadecanethiol and backfilled with 16-phenylhexadecane-1-thiol solution. As shown from the images, the square, where the arrow is pointing, at 2875 cm^{-1} showed a different contrast to when the IR is tuned to 3060 cm^{-1}. The pattern inverts contrast as the SFG probes CH_3 and phenyl, respectively; the square is dark when on resonance with the CH_3 group and bright

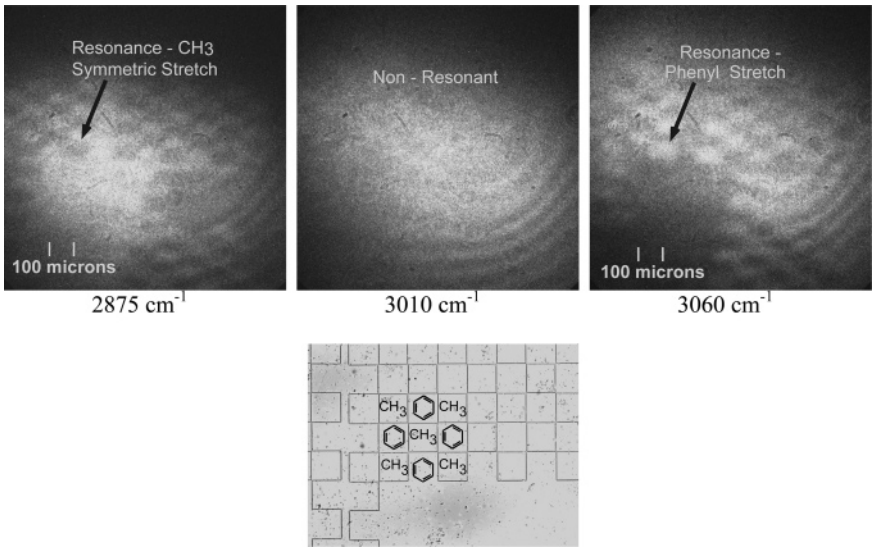

Figure 3. Pattern of CH_3-terminated and phenyl-terminated thiols in a checkerboard pattern. The image is 1 × 1 mm. Notice the defect region in the lower half of the image. The arrow indicates the same space on the surface. A representative visible light microscope image of the stamp used to make the pattern monolayer. Stamping and backfilling times are both 5 min.

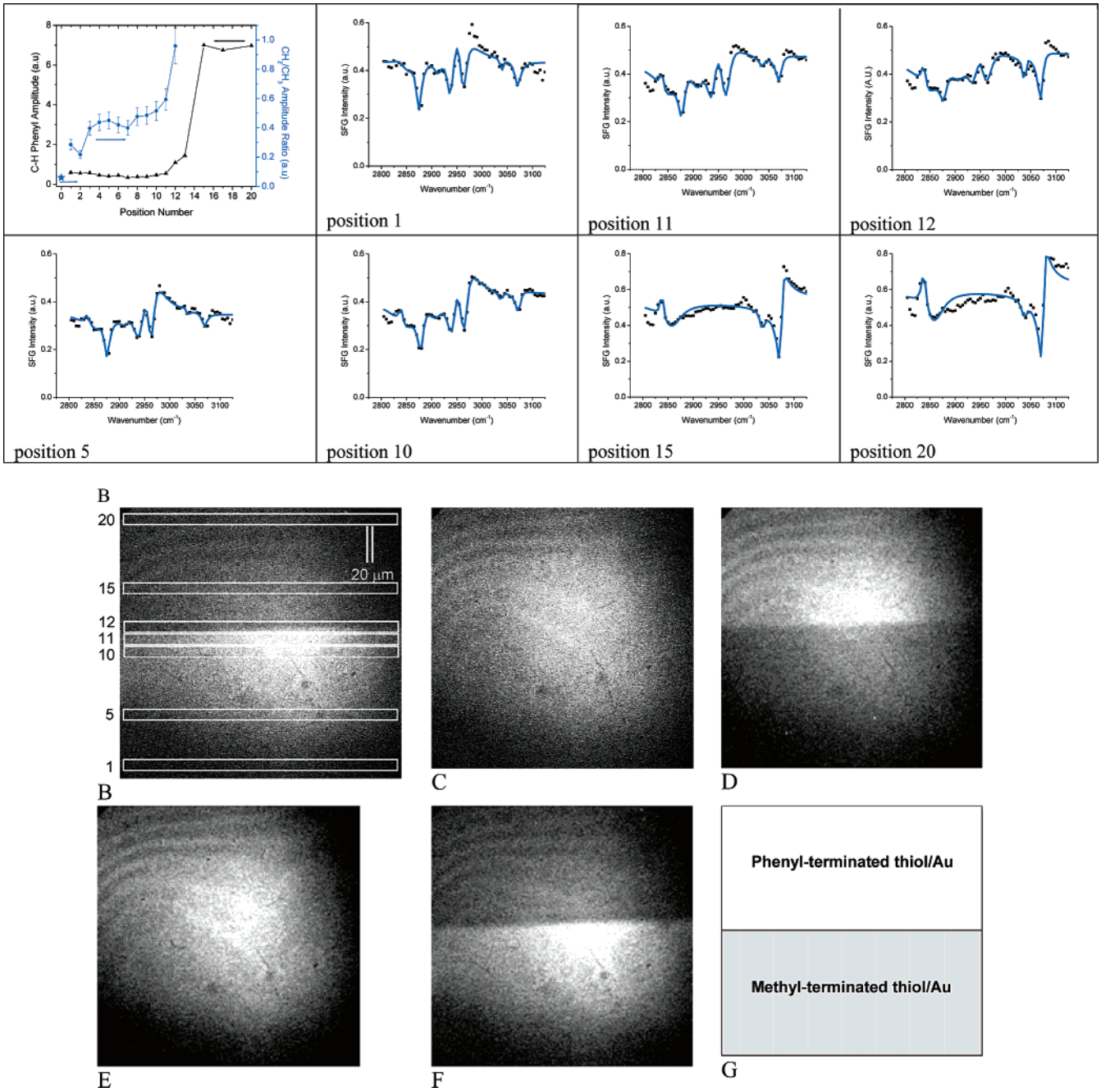

Figure 4. (A) SFG spectra in pp polarization of an edge patterned CH_3/phenyl monolayer taken at different positions of the image scanned from 2800 to 3100 cm^{-1}, position numbers on spectra correspond to those regions in Figure 4B. Also shown is a summary of the peak amplitude for the methyl and phenyl as a function of position on the surface. (B) SFG image of a CH_3-terminated stamped and a phenyl-terminated backfilled edge patterned monolayer. The outlined boxed regions correspond to the spectra shown in Figure 4A. The image in 4A is at 3060 cm^{-1}. (C−F) The images were taken at 2810, 2875, 2955, and 3060 cm^{-1} to represent nonresonant, resonant CH_3, and nonresonant and resonant phenyl contrast, respectively. The stamp and backfill times are 5 min each, respectively. (G) Represents the nominal location of the molecules in the printed surface.

when on resonance with phenyl, since the square contains mostly the CH_3-terminated monolayer. Also presented in Figure 3 is a visible light image of the stamp used to create the pattern in Figure 3.

How to Interpret SFG Images. The contrast in the SFG images, Figure 3, Figure 4, and Figure 7, is based on the resonance of the terminal groups in the monolayer (i.e., methyl or phenyl). These vibrational resonances occur as dips in the SFG spectra against the large nonresonant signal of the gold (see Figure 2 and eq 2).[42] Thus, a bright area of the image is due to the SFG signal from gold, and as the IR is tuned into the vibrational resonance of the molecule, the SFG signal decreases and the image becomes dark. This effect is the basis of the vibrational contrast in this SFG microscope and can differentiate the location of molecules on the surface since each molecule has a unique vibrational spectrum.

The edge pattern shown in Figure 4 is obtained by stamping, with CH_3-terminated C_{16} thiol, with a featureless PDMS stamp onto the gold substrate and then backfilling the stamped gold with phenyl-terminated thiol. SFG spectra were extracted from several positions across the sample from the "pure" CH_3-terminated to the phenyl-terminated hexadecane-1-thiol phase. Positions 1, 5, and 10 show predominantly CH_3 peaks, however there is noticeable intensity at ~3060 cm^{-1} due to the phenyl mode (discussed below). At positions 11 and 12, there are peaks observed due to both the phenyl and methyl

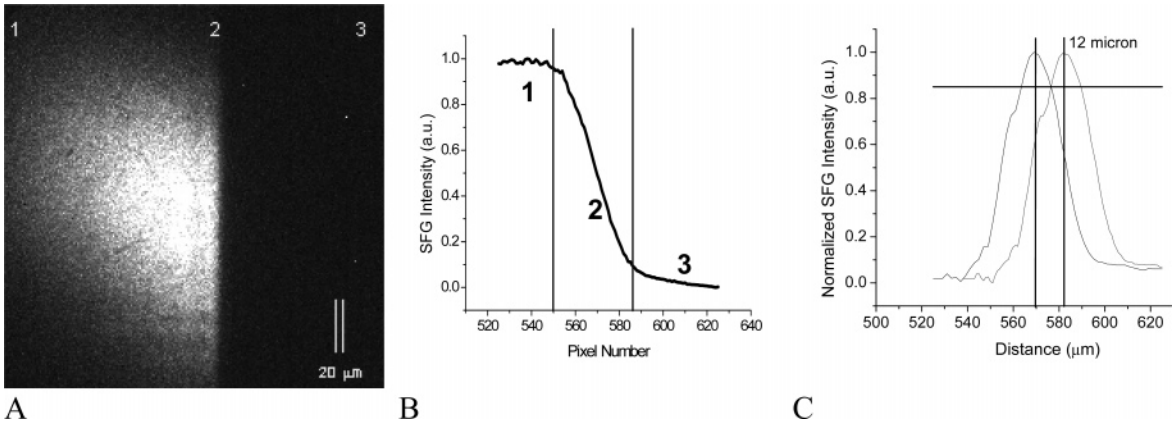

Figure 5. (A) SFG image of the gold/Si boundary. (B) Cross-section of the edge to estimate the resolution of the microscope. (C) Cross-section intensity profile of the surface.

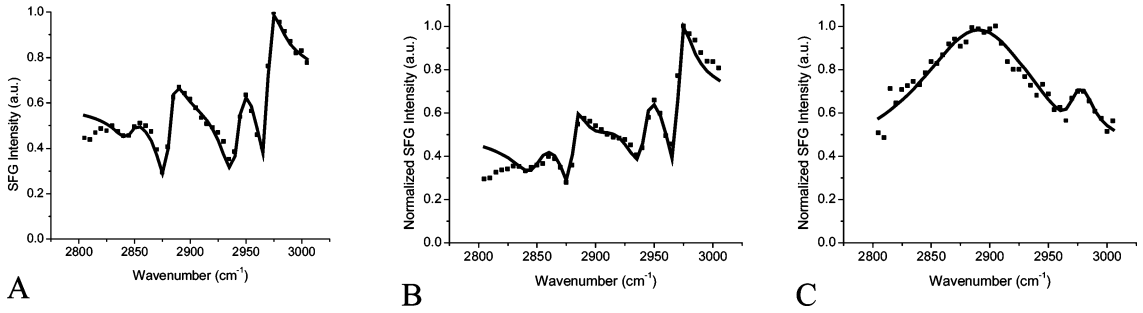

Figure 6. SFG spectra from regions 1, 2, and 3 of Figure 5A.

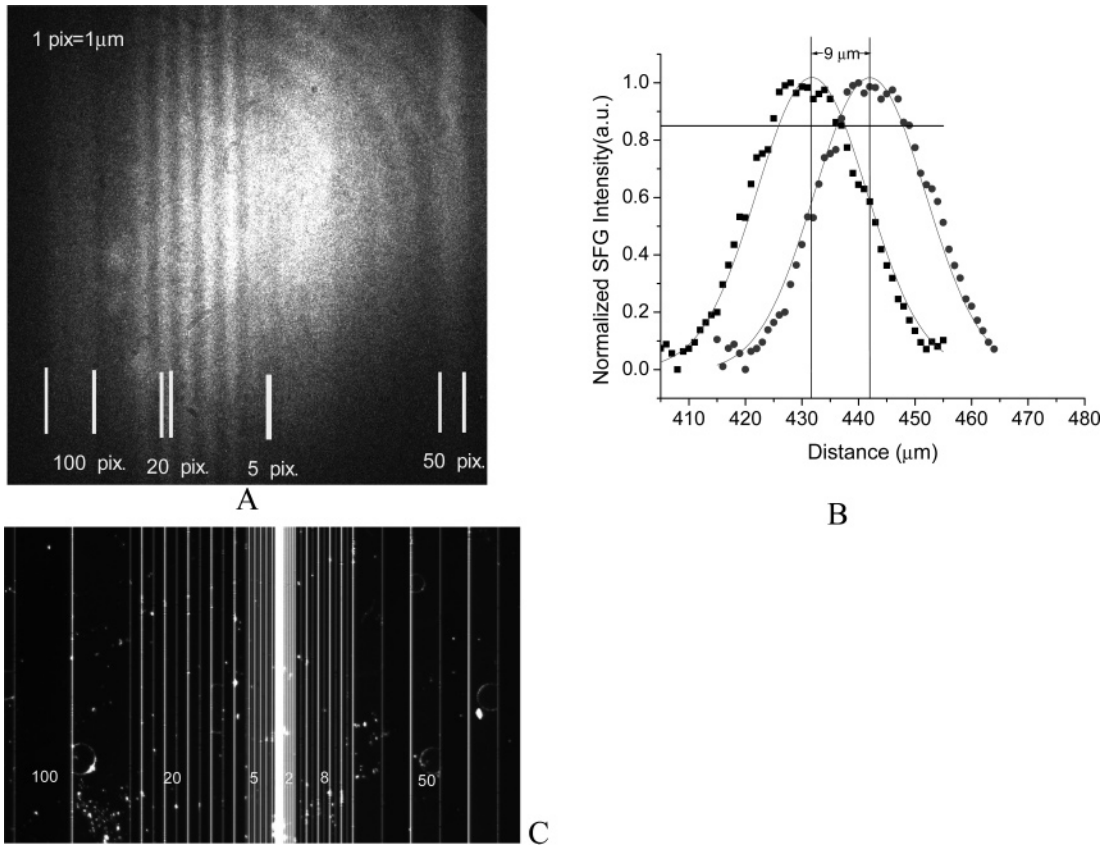

Figure 7. (A) Striped pattern of CH_3-terminated and backfilled with phenyl-terminated alkanethiols on gold, obtained at IR = 3060 cm^{-1}. (B) Cross-section of a 20 μm line. The solid line is a Gaussian fit. (C) Optical microscope image of the stamp master used for the pattern in Figure 7A, where the numbers indicate the feature width in micrometers.

groups, while at positions 15 and 20, only phenyl resonances are observed.

Mixing of Monolayers. Through the use of the above-mentioned analysis for contrast and resolution in the SFG

microscope, the spatial distribution of molecules in a microcontact-printed monolayer was analyzed. The image in Figure 4 demonstrates this point. The entire laser spot was imaged onto the CCD detector, and images were acquired in 5 cm^{-1} increments. Once these data were obtained, a postacquisition analysis was performed to extract the spectra from the different regions, shown as boxes in Figure 4B with the corresponding spectra in Figure 4A. There are three features to highlight from this figure: first, the backfilled monolayer (phenyl peak at $\sim$3060 cm^{-1}) appears in all of the spectra while the spectra of the pure phenyl region contain no methyl resonances. This observation suggests the mixing occurs during the backfilling step. Second, the SFG spectra at the boundary of the two phases contain a mixture of phenyl and methyl peaks, signifying increased mixing at the boundary of the two phases. Third, the SFG spectra of the CH_3 phase implies a mostly well-ordered densely packed monolayer based on the low intensity of CH_2 resonances.[48] Methylene peaks at 2850 and 2920 cm^{-1} are indications of gauche defects, which occur in less well-organized SAMs.[49] The spectra near the boundary indicate more CH_2 intensity and thus more defects (parts A and B of Figure 4, positions 10, 11, and 12). A plot of the symmetric stretch CH_2/CH_3 peak amplitude ratio and the C−H phenyl peak amplitude are shown in Figure 4A and indicate that, as the monolayer becomes more disordered, the phenyl peaks also increase in intensity and is interpreted as an increase in phenyl-terminated alkanethiol in the CH_3-terminated thiol stamped region due to the appearance of phenyl resonances in the CH_3 phase and the ease with which phenyl-terminated thiols are introduced into the CH_3 phase suggests that the overall monolayer formed by microcontact printing is less densely packed than those from solution-deposited films. This point is also suggested by comparing the CH_2/CH_3 ratio of a densely pack solution-deposited C_{16}-thiol surface to that of a printed C_{16}-thiol surface. (Note, the data point (★) at position zero in Figure 4A is the amplitude ratio for the solution-deposited C_{16} thiol, from Figure 2A.)

Despite the mixing of the backfilled molecules into the microcontact-printed area, good contrast is observed between the two phases. On the basis of the amplitude ratio of the phenyl peak in the two phases (assuming the orientation is the same) (Figure 4), the phenyl coverage in the CH_3 phase is about $^1/_{12}$ of that in the pure phenyl phase.

The image in Figure 5A is the boundary between a gold film with methyl-terminated C_{16}-thiol monolayer and the silicon wafer substrate. A cross-section is shown in Figure 5B along with the derivative to illustrate the resolution of the edge. The horizontal line is at 0.85 to indicate the Rayleigh criterion for resolution. Figure 6 displays the spectra taken in the thiol monolayer, the edge of the film, and at the Si wafer. The spectra in Figure 6 are representative of a relatively well-ordered monolayer, a disordered monolayer, and a "dirty" Si/SiO_2 surface, respectively. The CH_2/CH_3 symmetric stretch ratio for parts A and B of Figure 6 is 0.35 and 1.38, respectively (see Figure 4A for comparison).

A striped pattern of methyl-terminated, backfilled with phenyl-terminated thiols on gold is presented in Figure 7. The scale bars are indicated in Figure 7A. A cross-section of a 20 μm stripe is shown in Figure 7B with a Gaussian curve applied to the data points. The vertical lines indicate the peak center, and the horizontal line is at 85% of the max, which is used to indicate the Rayleigh criteria for resolution.

The above analysis is valid within the resolution of the current microscope design. The resolution is estimated in two experiments. In Figure 5, the contrast between the edge of the gold film and Si wafer substrate is used as a sharp boundary. The cross-section is shown in Figure 5B; the derivative of this profile is taken, and the Rayleigh criterion is applied to determine the resolving ability of the microscope.[50] The analysis indicates that the resolution is $\sim$12 μm (Figure 5C). Similarly, the resolution is estimated for a microcontact-printed monolayer in Figure 7. Application of the Rayleigh criteria to the cross-section gave a resolution of microscope under the condition of a mixed monolayer. Therefore, the current SFG microscope is able to obtain spatially resolved vibrational spectra of monolayers with a lateral resolution of $\sim$9 μm.

Contrast/Resolution of Microscope. The contrast in the SFG image arises from several factors, including instrumental and sample sources. The resolution of the microscope is estimated from the Abbe diffraction limit and is 1.7 μm for 800 nm SFG wavelength ($\sim$3100 cm^{-1} IR). A resolution of $<$1 μm is achieved for imaging the USAF Si mold with a HeNe laser at 632 nm with this microscope configuration.

For the SFG imaging, the real resolution is limited by the laser beams, magnification of the objective, pixel size of the CCD array and intensifier, and quality of optics in the signal path. Furthermore, the real resolution is limited by the sample quality, such as the quality of the gold substrate, molecules used in the printing, and molecular processes such as diffusion that will blur the boundaries between phases. Future experiments are aimed at optimizing these and exploring their importance in microcontact-printed monolayers.

Conclusions

This paper reports the results of a SFG microscope and its application to investigate the surface of microcontact-printed monolayers. The results indicate that there is significant mixing between the two regions of the pattern. Further, SFG spectra were obtained at different areas of the surface currently with a resolution of $\sim$10 μm.

Acknowledgment. We gratefully acknowledge the assistance of Mathilde Barriet, David Barriet, and Prof. Randy Lee for the thiol molecules, helpful discussions, and creating our first PDMS stamp. Also thanks to Alex Bittner and Klaus Kuhnke for inspiration in setting up this microscope. K.C. is supported by the Research Corporation.

References and Notes

(1) Xia, Y.; Whitesides, G. M. *Annu. Rev. Mater. Sci.* **1998**, *28*, 53.
(2) Xia, Y.; Whitesides, G. M. *Angew. Chem., Int. Ed. Engl.* **1998**, *37*, 550.
(3) Xia, Y.; Zhao, X.-M.; Whitesides, G. M. *Microelectron. Eng.* **1996**, *32*, 255.
(4) Miller, J. S.; Bethencourt, M. I.; Hahn, M.; Lee, T. R.; West, J. L. *Bio Eng.* **2005**.
(5) Lopez, G. P.; Biebuyck, H. A.; Whitesides, G. M. *Langmuir* **1993**, *9*, 1513.
(6) Noy, A.; Frisbie, C. D.; Roznyai, L. F.; Wrighton, M. S.; Lieber, C. M. *J. Am. Chem. Soc.* **1995**, *117*, 7943.
(7) Carpick, R. W.; Salmeron, M. *Chem. Rev.* **1997**, *97*, 1163.
(8) Kerimo, J.; Adams, D. M.; Barbara, P. F.; Kaschak, D. M.; Mallouk, T. E. *J. Phys. Chem. B* **1998**, *102*, 9451.
(9) Vanden Bout, D.; Kerimo, J.; Higgins, D. A.; Barbara, P. F. *Acc. Chem. Res.* **1997**, *30*, 204.
(10) Wilbur, J. L.; Biebuyck, H. A.; MacDonald, J. C.; Whitesides, G. M. *Langmuir* **1995**, *11*, 825.
(11) Zhou, Y.; Fan, H.; Fong, T.; Lopez, G. P. *Langmuir* **1998**, *14*, 660.
(12) Zharnikov, M.; Shaporenko, A.; Paul, A.; Golzhauser, A.; Scholl, A. *J. Phys. Chem. B* **2005**, *109*, 5168.
(13) Klauser, R.; Hong, I. H.; Wang, S. C.; Zharnikov, M.; Paul, A.; Golzhauser, A.; Terfort, A.; Chuang, T. J. *J. Phys. Chem. B* **2003**, *107*, 13133.

(14) Love, J. C.; Estroff, L. A.; Kriebel, J. K.; Nuzzo, R. G.; Whitesides, G. M. *Chem. Rev.* **2005**, in press.
(15) Wilbur, J. L.; Kumar, A.; Niebuyck, H.; Kim, E.; Whitesides, G. *Nanotechnology* **1996**, *7*, 452.
(16) Delamarche, E.; Schmid, H.; Bietsch, A.; Larsen, N. B.; Rothuizen, H.; Michel, B.; Biebuyck, H. *J. Phys. Chem. B* **1998**, *102*, 3324.
(17) Biebuyck, H. A.; Whitesides, G. M. *Langmuir* **1994**, *10*, 2790.
(18) Larsen, N. B.; Biebuyck, H.; Delamarche, E.; Michel, B. *J. Am. Chem. Soc.* **1997**, *119*, 3017.
(19) Cernusca, M.; Hofer, M.; Reider, G. A. *J. Opt. Soc. Am. B* **1998**, *15*, 2476.
(20) Florsheimer, M.; Raduge, C.; Salmen, H.; Bosch, M.; Terbrack, R.; Fuchs, H. *Thin Solid Films* **1996**, *284*−*285*, 659.
(21) Florsheimer, M.; Bosch, M.; Brillert, C.; Wierschem, M.; Fuchs, H. *Adv. Mater.* **1997**, *9*, 1061.
(22) Florsheimer, M. *Phys. Status Solidi A* **1999**, *173*, 15.
(23) Reider, G. A.; Cernusca, M.; Hofer, M. *Appl. Phys. B* **1999**, *68*, 343.
(24) Smilowitz, L.; Jia, Q. X.; Yang, X.; Li, D. Q.; McBranch, D.; Buelow, S. J.; Robinson, J. M. *J. Appl. Phys.* **1997**, *81*, 2051.
(25) Florsheimer, M.; Bosch, M.; Brillert, C.; Wierschem, M.; Fuchs, H. *J. Vac. Sci. Technol., B* **1997**, *15*, 1564.
(26) Potma, E. O.; Xie, X. S.; Muntean, L.; Preusser, J.; Jones, D.; Ye, J.; Leone, S. R.; Hinsberg, W. D.; Schade, W. *J. Phys. Chem. B* **2004**, *108*, 1296.
(27) Zumbusch, A.; Holtom, G. R.; Xie, X. S. *Phys. Rev. Lett.* **1999**, *82*, 4142.
(28) Cheng, J.-x.; Volkmer, A.; Book, L. D.; Xie, X. S. *J. Phys. Chem. B* **2001**, *105*, 1277.
(29) Cheng, J.-X.; Xie, X. S. *J. Phys. Chem. B* **2004**, *108*, 827.
(30) Cheng, J.-x.; Volkmer, A.; Book, L. D.; Xie, X. S. *J. Phys. Chem. B* **2002**, *106*, 8493.
(31) Hoffmann, D. M.; Kuhnke, K.; Kern, K. *Rev. Sci. Instrum.* **2002**, *73*, 3221.
(32) Kuhnke, K.; Hoffmann, D. M.; Wu, X. C.; Bittner, A. M.; Kern, K. *Appl. Phys Lett.* **2003**, *83*, 3830.
(33) Florsheimer, M.; Brillert, C.; Fuchs, H. *Langmuir* **1999**, *15*, 5437.
(34) Florsheimer, M.; Brillert, C.; Fuchs, H. *Mater. Sci. Eng., C* **1999**, *8*−*9*, 335.
(35) Hunt, J. H.; Guyot-Sionnest, P.; Shen, Y. R. *Chem. Phys. Lett.* **1987**, *133*, 189.
(36) Superfine, R.; Guyot-Sionnest, P.; Hunt, J. H.; Kao, C. T.; Shen, Y. R. *Surf. Sci.* **1988**, *200*, L445.
(37) Superfine, R.; Huang, J. Y.; Shen, Y. R. *Chem. Phys. Lett.* **1990**, *172*, 303.
(38) Baldelli, S.; Mailhot, G.; Ross, P. N.; Shen, Y. R.; Somorjai, G. A. *J. Phys. Chem. B* **2001**, *105*, 654.
(39) Lee, S.; Puck, A.; Graupe, M.; Colorado, R.; Shon, Y.-S.; Lee, T. R.; Perry, S. S. *Langmuir* **2001**, *17*, 7364.
(40) Baldelli, S. *J. Phys. Chem. B* **2003**, *107*, 6148.
(41) Bain, C. D. *J. Chem. Soc., Faraday Trans.* **1995**, *91*, 1281.
(42) Potterton, E. A.; Bain, C. D. *J. Electroanal. Chem.* **1996**, *409*, 109.
(43) MacPhail, R. A.; Strauss, H. L.; Snyder, R. G.; Elliger, C. A. *J. Phys. Chem.* **1984**, *88*, 334.
(44) Snyder, R. G. *J. Chem. Phys.* **1965**, *42*, 1744.
(45) Snyder, R. G.; Strauss, H. L.; Elliger, C. A. *J. Phys. Chem.* **1982**, *86*, 5145.
(46) Colthup, N. B.; Daly, L. H.; Wilberley, S. E. *Introduction to Infrared and Raman Spectroscopy*, 3rd ed.; Academic Press: San Diego, CA, 1990.
(47) Ward, R. N.; Duffy, D. C.; Bell, G. R.; Bain, C. D. *Mol. Phys.* **1996**, *88*, 269.
(48) Bohm, I.; Lampert, A.; Buck, M.; Eisert, F.; Grunze, M. *Appl. Surf. Sci.* **1999**, *141*, 237.
(49) Bain, C. D.; Davies, P. B.; Ong, T. H.; Ward, R. N. *Langmuir* **1991**, *7*, 1563.
(50) Hammond, C. *The Basics of Crystalography and Diffraction*, 1st ed.; Oxford University Press: New York, 1997.